Biophysical and computational approaches to study ternary complexes: A 'cooperative relationship' to rationalize targeted protein degradation

Jake A. Ward[1,a], Carles Perez-Lopez[1,a] and Cristina Mayor-Ruiz[1,*]

[1] Institute for Research in Biomedicine (IRB Barcelona), the BIST, Baldiri Reixac, 10, 08028 Barcelona, Spain
[a] Equal contribution
* Correspondence: cristina.mayor-ruiz@irbbarcelona.org

Abstract

Degraders have illustrated that compound-induced proximity to E3 ubiquitin ligases can prompt the ubiquitination and degradation of disease-relevant proteins. Hence, this pharmacology is becoming a promising alternative and complement to available therapeutic interventions (e.g., inhibitors). Degraders rely on protein binding instead of inhibition and, hence, they hold the promise to broaden the druggable proteome. Biophysical and structural biology approaches have been the cornerstone of understanding and rationalizing degrader-induced ternary complex formation. Computational models have now started to harness the experimental data from these approaches with the aim to identify and rationally help design new degraders. This review outlines the current experimental and computational strategies used to study ternary complex formation and degradation and highlights the importance of effective crosstalk between these approaches in the advancement of the targeted protein degradation (TPD) field. As our understanding of the molecular features that govern drug-induced interactions grows, faster optimizations and superior therapeutic innovations for TPD and other proximity-inducing modalities are sure to follow.

1. Introduction

1.1 Targeted protein degradation

Proximity-inducing pharmacology has become an important avenue of therapeutic intervention and it offers significant inroads to drug the "undruggable". Around 90% of human proteins, including many linked to life-threatening diseases, remain intractable via traditional inhibitors[1]. Recent advances in targeted protein degradation (TPD) illustrate that compound-induced proximity between an E3 ubiquitin ligase and a protein of interest (POI) can lead to ubiquitination and protein degradation, thus becoming a promising alternative for therapeutic intervention[2-5]. To date, most work on TPD has focused on chemically rewiring the ubiquitin-proteasome system (UPS) with compounds called "degraders" (Fig. 1a)[6-8]. Chemical modulation of protein abundance and improved selectivity are valuable features of this new therapeutic modality over the classical inhibitors.

Degraders can be monovalent or multivalent (typically bivalent, although trivalent degraders have also been developed[9]), depending on the number of distinguishable targeting moieties in the compound (Fig. 1a).

- Bivalent degraders are heterobifunctional molecules typically referred to as proteolysis targeting chimeras (**PROTACs**)[3] (Fig. 1a). They contain separate targeting moieties connected by a linker to engage both the target protein and E3 ligase. PROTACs generally have unfavorable druglikeness (their physicochemical property space falls beyond the "rule of 5"[10]). Nevertheless, an efficient in vivo effect can be achieved, and >15 PROTACs are currently in clinical trials[11].
- Monovalent degraders are linker-less molecules that induce the degradation of a POI by (i) gluing an E3 ligase (**molecular glue –MG– degraders**) (Fig. 1a) or by (ii) promoting a vulnerable target protein state that is then recognized by the proteolytic machinery of the cell (**destabilizers**)[6-7]. Of note, destabilizers may trigger protein degradation through autophagy rather than by the UPS[12]. Monovalent degraders can eliminate targets that are otherwise undruggable, they have advantageous drug-like properties, and they are already used in clinical practice (e.g., lenalidomide and analogs). However, their discovery and rational development are more challenging than PROTACs[6-7].

Over the past years, this growing field has moved from proof of concept to the development of degrader medicines in clinical trials. The advances in TPD have fueled interest in other proximity-inducing concepts that can trigger a plethora of outcomes in proteins and other biomolecules (such as RNA).

In this review, we share our thoughts on how biophysical and computational techniques, together with seminal structural information from crystallization and prediction studies, have shaped our current understanding of degrader-induced ternary complex formation and POI degradation. First, we discuss examples of useful approaches to characterize features of PROTAC and MG efficiency, leaving destabilizers outside the scope of this review. We start with biophysical techniques, followed by structural studies and computational approaches. Finally, we reflect on the utmost importance of a dynamic "conversation" and efficient integration of the data gathered by these strategies to maximize actionable information and further rationalize degrader designs.

1.2 Characterization and development of degraders: Principles of Ternary Complex Formation

Due to growing interest in the use of proximity-inducing agents for the treatment of disease, it has

become increasingly important to understand and characterize ternary complex formation. A ternary complex is formed by the interaction of three components. In the case of degraders, the ternary complex comprises an E3 ligase, a POI, and a degrader molecule. The formation of this complex is essential to induce ubiquitination and subsequent degradation of the POI. However, the process underlying this formation differs between the two types of degraders (PROTACs and MGs; Fig. 1b). A PROTAC molecule may first bind to either the E3 ligase or the POI before recruiting the other. In contrast, MGs typically form ternary complexes by a defined order[13]. For example, the MG may display affinity for one of the proteins involved, which alters the binding surface and promotes binding of the partner protein (e.g., FKBP12-Rapamycin-mTOR)[14].

Several features are used to describe the formation and productivity of small molecule-induced

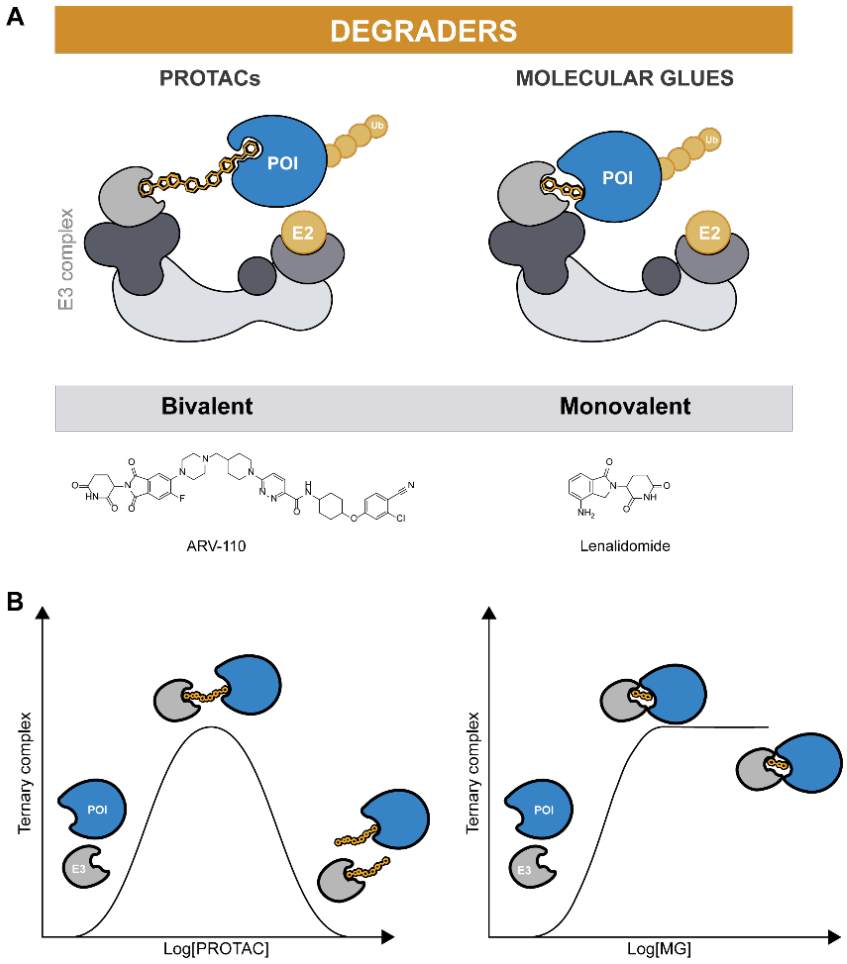

Figure 1. Types of degraders and induced ternary complex formation. A) Multivalent degraders (left, bivalent PROTACs are depicted). Monovalent degraders (right) comprise: molecular glue (MG) degraders and destabilizers. Only MGs degraders are shown. E3 schematics in PROTACs and molecular glue degraders represent an E3 of the Cullin RING ligase family. POI: protein of interest. B) Left: PROTAC-mediated ternary complex formation (and hook effect) as a function of PROTAC concentration. Right: MG-mediated ternary complex formation) as a function of MG concentration. POI (blue), E3 (gray).

ternary complexes. These include, but are not limited to, binding pose, affinity, cooperativity, stoichiometry, and residence time:

(i) The **binding pose** is a description of how each component (E3 ligase, degrader, and POI) comes together to form a ternary complex. PROTAC linker length, the ligandable protein sites, and the ways in which the two proteins can interact with each other determine the binding pose. The pose will ultimately determine whether the POI is successfully ubiquitinated and degraded. Structural determination of the ternary complex by X-ray crystallography is often used to characterize the binding pose. In addition, computational modeling can predict the most likely arrangement of the ternary complex (see Section 4).

(ii) **Affinity** is defined as the degree to which molecules (e.g., protein and ligand) bind to one another and it is frequently quantified by a dissociation constant (K_d); a lower K_d value indicates high affinity between the molecules. For PROTACs, each warhead has an affinity for target or E3. When the concentration of the PROTAC increases above the K_d^{binary} for each protein the additional PROTAC molecules preferentially form binary complexes resulting in a process known as the hook effect. As MGs often do not display measurable affinity for one or both of the proteins, the hook effect does not apply.

(iii) **Cooperativity** is a measure of the degree of additional affinity within the ternary complex compared with the individual binary affinities. Cooperativity, denoted α, is calculated by dividing the K_d^{binary} by the $K_d^{ternary}$. Cooperativity is positive when $\alpha > 1$, indicating that the formation of a ternary complex is favorable due to, for example, the formation of additional interactions at the protein-protein interface. A value < 1 indicates negative cooperativity, meaning that the formation of the ternary complex is unfavorable, for example, because of steric clashes. When the K_d values for the binary and ternary complexes are equal (the α value is 1), the system is said to be non-cooperative. For PROTACs, positive cooperativity can ensure selectivity, allow for the use of weak ligands, and improve degradation efficiency[15-19]. Nevertheless, non-cooperative PROTACs can also elicit potent degradation[20-21]. MG degraders depend on the formation of highly cooperative ternary complexes for their activity as they often display weak binding affinities to one or both of the proteins implicated.

(iv) Generally, the binding **stoichiometry** of degrader-induced ternary complexes is 1:1:1 (E3:degrader:POI). The catalytic mode of action of degraders via ternary complexes allows for the dosing at substoichiometric concentrations to elicit degradation of the POI.

(v) Finally, **residence time** is the duration that the components are assembled into the ternary complex. Residence time is dependent on the rate of dissociation of the complex (k_{off})[22].For degraders, a sufficiently slow k_{off} is required to allow time for POI ubiquitination to occur[23].

A range of in vitro and in cellulo strategies have been employed to characterize the mechanism of action of degraders. These assays provide vital information such as the affinities, thermodynamics, kinetics, and binding pose governing ternary complex formation as well as the POI degradation profile. Together with structural information from crystallization and prediction studies, the data obtained from these approaches can be used to design and validate computational models for degrader design. The degraders predicted can then be tested in vitro and in cellulo to confirm their effectiveness. The technologies most frequently used are discussed in more detail in the next sections.

2. Biophysical Methods to Study Ternary Complex Formation

2.1 In vitro

2.1.2 Proximity-based assays: TR-FRET and AlphaScreen

Time-resolved fluorescence energy transfer (TR-FRET) and amplified luminescent proximity homogeneous assays (AlphaScreen / AlphaLISA) are routinely used to characterize the formation of a ternary complex and to determine the concentration range at which these complexes are generated. Both assays measure the energy transfer between a donor and an acceptor species when in close proximity. To study ternary complex formation, the compound of interest is often titrated into a system containing a fixed concentration of the two POIs. The increasing concentration of the compound leads to a higher population of the ternary complex and subsequently a higher output signal, until a maximum is reached. For MG degraders, parameters such as EC_{50} and the maximum response achieved (E_{max}) provide information on potency and cooperativity[24]. For example, TR-FRET was used to study Helios MG degraders[24].

In the case of PROTACs, a characteristic bell-shaped curve is observed, where the concentration of the ternary complex decreases at high PROTAC concentrations as a result of the hook effect. The response curves obtained can also be used as an indication of the cooperativity of the PROTAC-induced ternary complex. A more cooperative PROTAC forms a larger population of ternary complexes, resulting in a higher maximal peak intensity over a broader concentration range[15, 25]. Examples of the use of TR-FRET and AlphaScreen assays to investigate PROTAC-induced ternary complexes include the study of CRBN-recruiting PROTACs for BTK[20] and BET bromodomains[26-27] and

VHL-recruiting PROTACs of BRD7/9[21]. Recently, Du *et al.* (2022) used TR-FRET assays to explore the target scope of KEAP1 E3-based PROTACs[28].

Proximity-based assays can also be used to gather further information about ternary complex formation, such as the values of cooperativity and binary and ternary K_d. To study MG-induced ternary complex formation, one of the POI is titrated to a fixed concentration of the other in the presence and absence of the MG. Simonetta *et al.* (2019) used TR-FRET to characterize small molecules that enhance the interaction between the E3 $CRL1^{\beta\text{-}TrCP}$ and mutant β-catenin[29]. They titrated a β-catenin peptide to a fixed concentration of the substrate receptor β-TrCP in the absence and presence of different concentrations of a small molecule, namely NRX-1532[29]. In the presence of ≥ 250 μM NRX-1532, the affinity for β-Catenin and $CRL1^{\beta\text{-}TrCP}$ was increased by a factor of 10, thus indicating that maximum cooperativity (α = 10) was reached at this concentration[29]. A similar strategy has also been employed to study the ternary complex formation orchestrated by IMiDs[30], cyclin K MGs[24, 31] (Fig. 2), and aryl sulfonamides[32].

To determine values for binding and cooperativity, the classic bell-shaped curve observed in direct binding assays for PROTACs is difficult to deconvolute. Therefore, competition-based proximity assays can be used. Farnaby *et al.* (2019) used a TR-FRET competition assay to measure the displacement of a fluorescent SMARCA2 probe by the PROTAC ACBI1 in the presence and absence of VHL (VBC)[33]. The displacement of the fluorescent probe, bound to fluorescently labeled SMARCA2, resulted in a decay in the FRET signal, which was plotted against the concentration of ACBI1 alone (binary) and ACBI1-VCB (ternary). Cooperativity was then determined by calculating the ratio of the binary and ternary K_d values[33].

Proximity-based assays (AlphaScreen and TR-FRET) are high-throughput, sensitive and homogenous techniques to directly measure ternary complex formation in vitro *(FRET has also been applied in cellulo, as discussed in section 2.2.2)*. In TR-FRET, the donor species has a fluorescence lifetime that is considerably longer than the background fluorescence, reducing the potential compound interference[34]. However, compounds can lead to fluorophore quenching, resulting in false negative results. In AlphaScreen assays, compound interference can occur from quenching of the singlet oxygen generated upon excitation of the donor bead. TR-FRET assays typically have a narrower dynamic range, lower theoretical proximity limits and higher assay variability when compared with AlphaScreen assays[34-35]. For AlphaScreen assays, careful consideration is required to avoid prolonged exposure to ambient light and changes in temperature to avoid assay variability. Other techniques can be used as orthogonal assays to verify the results from these proximity-based approaches and to

provide key information on the thermodynamics and kinetics of ternary complex formation.

2.1.2. Fluorescence polarization

Fluorescence polarization (FP) has also been employed to study ternary complex formation. FP can be used to determine the cooperativity and potency of MGs. The typical assays require titration of an unlabeled POI to a fixed concentration of a labelled binding partner in the presence and absence of the MG. This approach is similar to that followed in TR-FRET and it has frequently been applied to profile MG stabilizers for the 14-3-3 family of proteins[36-37]. A second approach involves titrating the MG to a fixed concentration of the labelled and unlabeled proteins to determine potency (EC_{50})[29, 37]. Competitive displacement assays using FP have also been used to deconvolute the events underpinning PROTAC-induced ternary complex formation[33, 38-39]. In these assays, displacement of a bound fluorescent probe results in a loss of polarized flourescence. To determine inhibitory values (apparent K_d) and cooperativity, the change in this parameter is plotted against the concentration of the POI that is titrated.

FP has the advantage over proximity-based assays in that it requires the labeling of only one protein and its design is simpler. However, FP assays require a change in the tumbling rate of the fluorescent molecule upon binding and they are limited by the affinities than can be measured. Furthermore, compounds that have intrinsic fluorescence or lead to quenching of the fluorophore can result in false positive or negative results, respectively. Nevertheless, as a high-throughput technique, FP has been used to screen large numbers of potential MGs[36, 40].

191

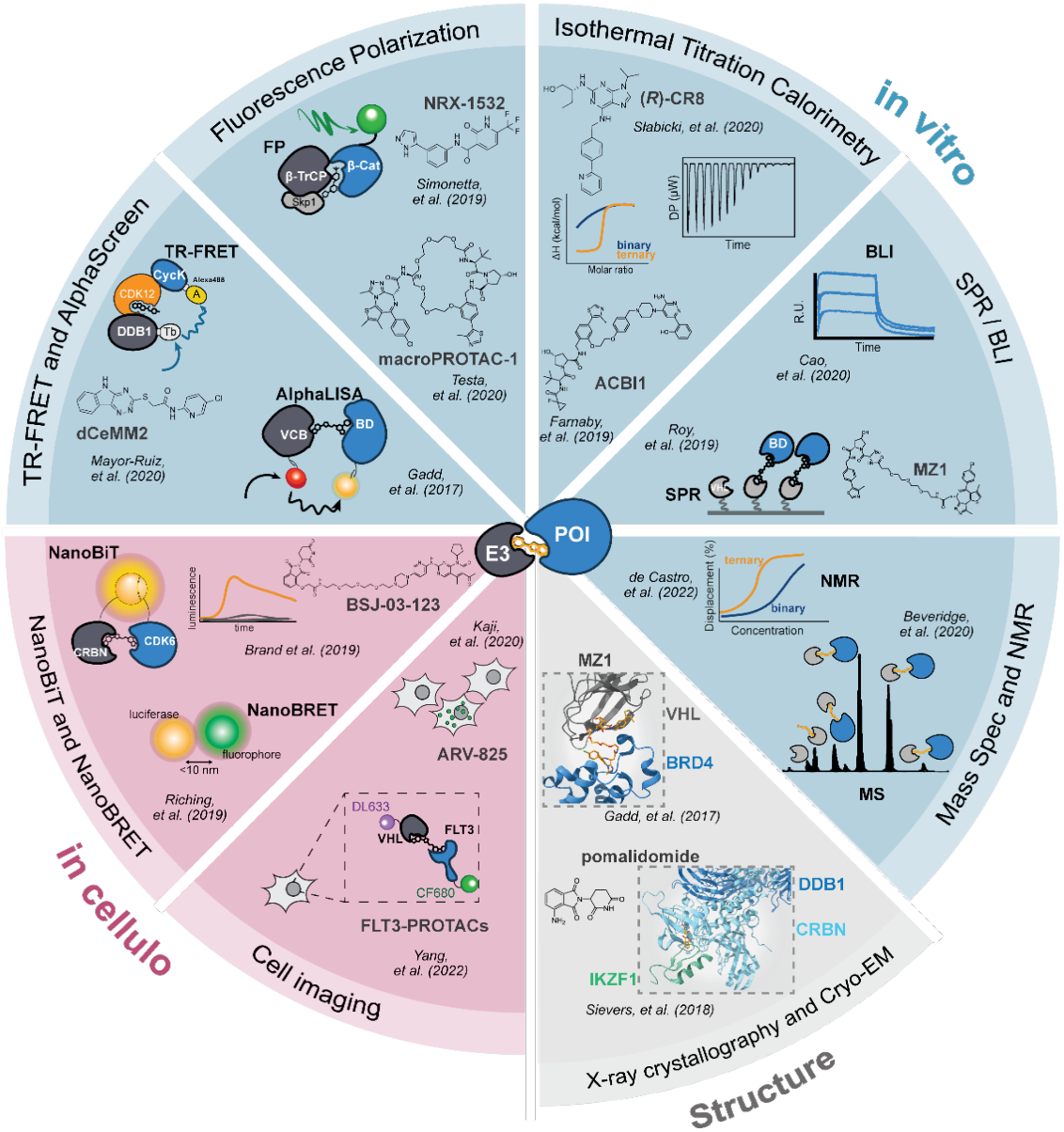

Figure 2. Exploring and characterizing ternary complex formation. *Depiction of the principal in vitro and in cellulo strategies used to study ternary complex formation. The following information is provided: technique used, a representation of the assay design and the readout, the chemical structures of key compounds and key paper references. BD: bromodomain. BLI: bio-layer interferometry. Cryo-EM: cryogenic electron microscopy. The X-ray crystal structures of the DDB1-CRBN-pomalidomide IKZF1 complex and the VHL-MZ1-BRD4 complex are shown (PDB: 6H0F and 5T35, respectively). AlphaLISA: amplified luminescent proximity homogeneous assay. FP: fluorescence polarization. MS: mass spectrometry. NanoBRET: Nano-bioluminescent resonance energy transfer. NMR: nuclear magnetic resonance. SPR: surface plasmon resonance. TR-FRET: time-resolved fluorescence energy transfer. R.U.: response units. DP: dynamic potential. POI: protein of interest. VCB: the complex of VHL with Elongin B and C.*

192

193

2.1.3 Isothermal Titration Calorimetry

Isothermal Titration Calorimetry (ITC) is a label-free, in-solution, and direct method that can be used to study the thermodynamics of ternary complex formation. ITC can provide information on the associative and dissociative binding constants (K_a and K_d, respectively), the binding stoichiometry (N) and changes in enthalpy (ΔH), entropy (ΔS) and Gibb´s free energy (ΔG).

For MGs, the common strategy is to titrate one of the proteins in the syringe into the other (in the cell), in the presence and absence of the compounds. A reduction in the K_d value (higher affinity) is used as an indication of the stabilization of the ternary complex, and the thermodynamic profile (ΔH and ΔS) provides information as to the driving force for the formation. ITC was used to show that CR8 acts as a MG for DDB1 and CDK12-Cyclin K[41] (Fig. 2). The thermodynamics revealed that a more favorable ΔH was the main contributing factor to the formation of a stable ternary complex (more negative ΔG)[41] (Fig. 2). ITC has been more readily used to study ternary complex formation induced by non-degradative MGs. A key example is given by the stabilization of 14-3-3 protein interactions by the natural product Fusicoccin A[37, 42].

For the characterization of PROTACs, titration of these compounds in the syringe into the POI in the ITC cell would be expected to result in competing equilibria due to the hook effect. Therefore, for these assays the PROTAC is placed in the cell[15]. Farnaby *et al.* (2019) used ITC to study VHL-recruiting PROTACs for SMARCA2[33] (Fig. 2). First, the VHL (VCB) was titrated into the PROTAC to ascertain the K_d^{binary}. Next, VCB was titrated into a saturated SMARCA2-PROTAC complex to determine the $Kd^{ternary}$ and subsequently the cooperativity[33] (Fig. 2). A similar strategy has been employed to study VHL Homo-PROTACs[16] and VHL-recruiting PROTACs for $BRD4^{BD2}$ [18, 39].

ITC has also been used to study PROTAC selectivity and to optimize PROTAC design. Zoppi *et al.* (2019) used ITC for the characterization of optimized VHL-recruiting PROTACs against BRD7/9[21]. The ITC data helped explain that the limited degradation of BRD7/9 for a first-generation PROTAC was due to negative cooperativity. The thermodynamics revealed that the ternary complex was less stable than the binary complexes, predominantly because of an unfavorable ΔS contribution[21]. Based on these results, the authors synthesized second- and third-generation PROTACs that showed greater cooperativity. In addition, the most thermodynamically stable ternary complex *in vitro* resulted in potent and rapid degradation in cells[21].

Additional ITC experiments can be conducted to provide further information about the events contributing to the induced ternary complex. These include, for example, titration of a MG into either protein to determine binary K_d values or to a complex of both proteins to determine EC_{50}[43]. In

addition, it is important to conduct the appropriate control titrations in ITC, for example, to eliminate the heat associated with dilution.

ITC is relatively low-throughput and often requires considerable amounts of material, thereby making it unsuitable for studying large numbers of compounds. Nevertheless, ITC can provide a detailed characterization of ternary complex formation that support in cellulo data such as degradation efficiency.

2.1.4 Surface Plasmon Resonance and Bio-layer Interferometry

As well as thermodynamics, the kinetics of ternary complex formation is an important consideration in the characterization and optimization of degraders[44]. Surface Plasmon Resonance (SPR) is a label-free inhomogeneous technique than can be used to determine binding parameters (K_a and K_d and subsequently cooperativity), stoichiometry, and kinetics (association (k_{on}) and dissociation (k_{off}) rate constants). Furthermore, it can also be used to determine the Gibb´s free energy (ΔG) as a description of the stability of the binary and ternary complexes. As SPR can be conducted at different temperatures, the enthalpic (ΔH) and entropic (ΔS) contributions can be determined by a Van´t Hoff Plot[45].

Roy *et al.* (2019) reported the first SPR assay to measure the kinetics of ternary complex formation involving the PROTAC MZ1[38] (Fig. 2). First, MZ1 was titrated into VHL immobilized on a sensor chip. Next, the MZ1 PROTAC, pre-incubated with near-saturating concentrations of target protein, was titrated to VHL[38]. The VHL/MZ1/BRD4^{BD2} ternary complex had the fastest k_{on} and the slowest k_{off} when compared with other VHL-recruiting PROTACs for BRD4^{BD2}, thereby explaining the significant positive cooperativity[38]. SPR was also used to quantify and compare the kinetics of VHL/PROTAC/BD2 ternary complexes for each bromodomain[38]. Most importantly, the authors noted a correlation between the BET bromodomains with the shortest-lived ternary complexes (shortest half-life ($t_{1/2}$)) and the slowest rate of degradation in HEK293 cells. A similar strategy has also been followed to study VHL-recruiting PROTACs against BRD4^{BD1} [46], SMARCA2[47] and p38[48] and CRBN-recruiting PROTACs for BTK[20].

Ternary complex formation induced by non-degradative MGs has also been studied by SPR[49-50]. Guillory *et al.* (2020) used SPR to show that the small-molecule fragment AZ-008 increases the affinity between 14-3-3 protein and a phosphorylated peptide mimicking the C-terminus of the tumor suppressor protein, p53[49]. For this assay, 14-3-3 protein was titrated into immobilized p53 peptide in a multi-cycle format in the presence and absence of AZ-008[49].

Recently, bio-layer interferometry (BLI) has been successfully used to study ternary complex formation[51-52]. BLI yields similar information as SPR on the affinity and kinetics of ternary complexes. However, BLI uses biosensors for protein immobilization and a ´dip and read´ technology to measure binding, rather than the continuous sample flow used in SPR. The ´dip and read´ technology of BLI offers more user convenience and is more amenable to using cell lysates. However, BLI has reduced sensitivity when compared with SPR. Cao *et al.* (2022) used BLI to characterize ternary complexes induced by different MGs (CBD, IMiDs and auxin)[52] (Fig. 2).

SPR and BLI allow for thorough characterization of ternary complex formation (affinity, kinetics and thermodynamics) in a high-throughput manner and with lower sample demand than ITC. However, as these techniques require immobilization of one of the proteins being studied, careful consideration is required to avoid any impairment on binding.

2.1.5 Other techniques to study binary and ternary complex formation

As well as those outlined above, additional techniques have been used to study binary and ternary complex formation. These include dynamic scanning calorimetry[43, 53], size-exclusion chromatography[16, 23, 54] microscale thermophoresis (MST)[55], native mass spectrometry[56-58], and nuclear magnetic resonance (NMR)[51, 59]. These techniques serve as orthogonal assays to the main strategies such as TR-FRET and SPR, but they can also provide additional advantages. For example, native mass spectrometry allows for the study of intermediate states involved in complex formation. In addition, this technique can be used to study preferentially formed ternary complexes from multicomponent mixtures in a single experiment, making it an attractive approach for high-throughput screening[56-57]. However, while native mass spectrometry allows for the assessment of the efficiency of PROTAC- or MG-induced ternary complex formation, it does not provide values for thermodynamic nor kinetic parameters.

In vitro biophysical assays give useful insights into the characteristics of ternary complex formation. However, they do not provide an adequate representation of the complex cellular environment nor do they take into account factors that affect compound exposure, such as permeability, compound efflux, compound sequestration, or metabolism. Therefore, it is paramount to assess whether the formation of a ternary complex is recapitulated in cellulo.

2.2 In cellulo

Ternary complex formation in intact cells can be studied using technologies such as NanoBRET[21, 41, 60-62] and NanoBiT[54, 63], as well as by cell imaging techniques (e.g. phase-shift live cell imaging[64-65]).

Furthermore, other approaches, namely co-immunoprecipitation[66], chemo-proteomics[31], cellular thermal shift assay (CETSA)[48, 53, 67], in-cell NMR[68], and FP[69] can be used to address target engagement in lysates or in cells.

2.2.1 NanoBRET and NanoBiT

Nanobioluminescent resonance energy transfer (NanoBRET) is a proximity-based assay that measures the fluorescence signal emitted from an acceptor fluorophore (e.g. HaloTag-conjugated protein labeled with 618 ligand; the HaloTag is a 33 kDa protein that can be covalently modified with a synthetic ligand such as a fluorophore)
when in close proximity to the donor (Nanoluciferase-tagged protein) and in the presence of luciferase substrate[70]. As with in vitro proximity-based assays, the presence of a compound that induces ternary complex formation will result in an increase in luminescence signal as the two proteins are brought within proximity. Furthermore, monitoring BRET ratio over time can be used to follow the kinetics of ternary complex formation, and the displacement of fluorescently labeled tracers can be used to measure target engagement in live cells[60, 62]. Interestingly, Riching *et al.* (2018) used nanoBRET to relate the stability of PROTAC induced ternary complex formation with degradation in live cells for the VHL-MZ1-BET bromodomain systems[60]. Since then, this approach has been used to study VHL-recruiting PROTACS for BCL-XL[61] and the Cyclin K MG degrader CR8[41], among others.

An orthogonal assay to NanoBRET is the NanoLuc Binary Technology (NanoBiT®). This approach uses tagging of the E3 and POI pair, each with a subunit of the nanoluciferase enzyme (NanoBiT)[71] (Fig. 3). The two subunits (LgBiT and SmBiT) display low affinity (K_d = 190 μM) and therefore the interaction of the E3 and the POI drives the LgBiT-SmBiT interaction. Due to weak affinity between the sub-units, the NanoBiT system cannot detect protein-protein interactions weaker than the interaction between LgBiT and SmBiT. NanoBiT technology has been used to study VHL-recruiting PROTACs for BCR-ABL[54] and BRD4[63] and selective CRBN-recruiting PROTACs against CDK6[72] (Fig. 3), among others.

2.2.2 Cell imaging

Cell-imaging approaches have also been applied to study ternary complex formation in real time. These include fluorescence imaging techniques such as SPPIER[64], FLOUPPI[65], and dSTORM[73] (Fig. 2). For example, separation of phase-based protein interaction reporter (SPPIER) was used to show the IMiD-induced ternary complex formation involving CRBN and IKZF1[64] (Fig. 2). Other techniques such as FRET[74-76]and PLA[77] have also been applied to examine protein-protein interactions in cells and could potentially be used to address ternary complex formation in the TPD field.

2.3 Monitoring Protein Degradation in Cells

The effectiveness of a degrader is ultimately determined by its capacity to elicit the degradation of a POI. Such capacity cannot be determined solely by studying the formation of a stable ternary complex. For example, the POI must be positioned in an orientation such that lysine residues are accessible for ubiquitin transfer. Therefore, having robust methods available to study protein degradation and resynthesis of the POI in cells is vital in the assessment of degraders.

A well-established method to study protein degradation is western blotting, which allows for the semi-quantitative measurement of protein levels[53]. However, this technique relies on access to specific antibodies and it has limited sensitivity. Additional immunoblotting methods (e.g. capillary electrophoresis[47], ELISA[66] and immunofluorescence[78]) and mass spectrometry[20, 24, 31, 67, 72] have improved the quantification and sensitivity of determining protein levels. A key advantage of mass spectrometry analysis over immunoblotting methods is that it allows measurements of changes across the proteome. However, all of these techniques have a relatively low-throughput. The development of a TR-FRET-based assay that uses primary antibodies targeting the POI and the E3 has improved the scalability and sensitivity of immunoblotting techniques, without the need of protein tagging[79].

The development of reporter assays has allowed for the real time monitoring of protein degradation and resynthesis in cells. These approaches include fluorescent conjugates (e.g., GFP)[41, 80-82] and split luciferase tags such as Promega's HiBiT[60]. For the HiBiT assay, the POI is fused to an 11 amino acid tag known as HiBiT that interacts with a larger subunit (Large BiT; LgBiT) and then emits luminescence in the presence of a substrate[60]. For these reporter assays, careful consideration is required to ensure that tagging does not affect the stability or function of the protein.

Dose-response and time-course experiments with reporter systems provide key information, such as rates of degradation and resynthesis, the maximal degradation achieved (D_{max}) and the concentration that induces half-maximal degradation (DC_{50})[60]. Interestingly, Kristin *et al.* (2018) developed a Nano-BRET assay to simultaneously measure ternary complex formation and degradation[60]. For this assay, they used the HiBiT-BET protein complemented with LgBiT as an energy donor and Halo-Tag fused to an E3 ligase as the energy acceptor[60]. Among others, this approach has also been used to study VHL-recruiting PROTACs for WDR5[83].

3. Structural Determination of Ternary Complexes

By providing vital information on the binding pose, structural determination of the ternary complex assists in rationalizing the observed behaviors of degraders. X-ray crystallography is the most frequently used technique for structural determination. The first degrader-induced ternary complex was solved by Gadd *et al.* in 2017 for VCB-MZ1-BRD4^{BD2} and, since then, over 20 structures have been deposited in the Protein Data Bank (PDB)[15]. Cryogenic-electron microscopy (Cryo-EM) [32, 43, 84-85] and Small Angle X-Ray Scattering (SAXS)[86] have also been used to elucidate the ternary complex formation induced by MG degraders and PROTACs. Importantly, structural information on the binary and/or ternary complexes is utilized to develop computational models and to train predictions. Approaches such as homology modeling or artificial intelligence-driven structural predictions (e.g., Alphafold[87] or RosettaFold[88]) can predict the structures of individual proteins. Other methods like Alphafold Multimer[89] can produce high-accuracy binary protein complexes. When structural information is not available, all these tools may be useful in the future to help predict degrader-induced ternary complexes.

4. Computational Modeling

Computational modeling is a strategy that uses 3D structural data to mimic the behaviors of a given molecule, such as ligand-protein binding processes. Therefore, high-quality experimental data is fundamental. In recent decades, biophysical data have provided critical information to describe protein-ligand and protein-protein binding events, which is strongly needed for the training and improvement of modeling tools. However, the drug-induced proximity rationale has changed the binding paradigms behind these methods. New data and the modification of the current strategies have been necessary to adapt these methods to the TPD field.

4.1 Key computational techniques in TPD

In recent years, multiple computational methods have been developed to characterize and predict native-like ternary complexes. These techniques usually consist of complex pipelines that integrate and tune modeling tools that were originally designed for other purposes, adapting their application to TPD. In the next subsections, we will review some of the most relevant tools that have been applied, integrated, and/or adapted to model ternary complex formation and subsequent degradation of the POI. Most of the available examples focus on PROTAC-induced ternary complex and, thus, PROTACs will be our focus.

4.1.1 Structure generation techniques

Protein-protein docking

Accurate prediction of binary protein complexes is required to obtain truthful models of drug-induced ternary complexes. These algorithms aim to generate complexes from two individual proteins (Fig. 3). First, adequate translations and rotations are required, typically following a rigid-body approach. After this step, protein-protein docking methods rank and score the complexes generated[90-92].

Schiedel *et al.* (2018) pioneered the integration of protein-protein dockings with HADDOCK[93] to rationalize PROTAC-induced degradation[94]. Nowak *et al.* (2018) utilized Rosetta[95] to model the possible binding modes of CRBN on $BRD4^{BD1}$ [25]. Rosetta has become one of the most widely used protein-protein docking techniques in TPD. Alternative tools applied in TPD include PatchDock[96-97], FRDOCK[98-99], MOE packages[100-103], ClusPro[104], and LightDock[105]. The in silico determination of ternary complexes calls for a thorough understanding of protein-protein conformations. However, resolving ligand (PROTAC) geometry is also needed to create accurate models, as discussed in the following section.

Ligand/PROTAC Conformational Sampling

Ligand-induced ternary complexes via bivalent molecules, such as PROTACs, involves sequential binding to the E3 or POI first, followed by subsequent binding to the other protein. Therefore, sampling the ligand conformations is important to adapt the PROTAC to the new protein-protein poses. To this end, available methods apply different algorithms to rotate the bonds of the ligand. These rotations can be limited to avoid clashes with the protein (anchored sampling) or in solvent-like conditions (free sampling) (Fig. 3). In addition, some parts of the molecule can be constrained (Fig. 4). Ligand docking can also generate ligand geometries around the protein-binding site and score them. For example, Schiedel *et al.* (2018) used GOLD to generate ligand poses on conformations obtained from protein-protein docking[94]. Without available protein crystals, ligand docking can provide starting orientations for the E3 and POI [100]. For instance, Zhu *et al.* (2022) used Glide docking from the Schrödinger Suite to dock the POI-binding moiety into the AKT binding site and used this structure as the starting point for the in silico modeling[106].

Once the ligand conformations are produced, docking scoring functions can be used to evaluate the ligand energy. For instance, Weng *et al.* (2021) incorporated Autodock Vina to assess the binding energy of PROTAC conformations[98]. The integration of protein-protein docking with ligand conformational sampling methods can lead to the formation of potential ternary complexes.

Molecular dynamics (MD)

Proteins are dynamic, a property that is particularly relevant when predicting ternary complexes. Rigid-body approaches such as docking are unable to capture the protein-ligand induced-fit effects

or apo-holo (unbound-bound) state conformational changes. Molecular dynamics (MD) can assist in solving such rigidity-related problems. MD relies on the application of Newton's equations to introduce forces and recalculate the location of each atom in the system as a function of time (Fig. 3). By iterating these steps, one can produce "movies" showing the motion of the system for a specific length of time, from a few femtoseconds to milliseconds[107].

MD simulations have been widely used to develop traditional inhibitors[108] and non-degradative bivalent compounds[109-111]. Smith *et al.* (2019) used MD simulations to asses two distinct ternary complex conformations for two VHL-recruiting PROTACs against p38δ (SJFα and SJFδ)[48]. The comparative protein-protein interactions between models explained the selectivity of SJFδ for p38δ over SJFα[48]. Bondeson *et al.* (2019) also used MD for the VHL-p38α complex after docking of the PROTAC 1, and then assessed the stability of the system[112]. Furthermore, Testa *et al.* (2020) used MD to evaluate two cyclic derivatives of the PROTAC MZ1[39]. These results guided the design of the macrocyclic macroPROTAC-1[39] (Fig. 2).

Regarding ligand conformational sampling, Weerakoon *et al.* (2022) used MD simulations to study the conformational behavior of MZ1 and dBET6 and correlated the results with NMR data[113]. Interestingly, Dixon *et al.* (2022) modelled the entire ternary complex formation for the VHL-recruiting PROTAC ACBI1, in the SMARCA2^{BD2} system, by integrating MD with hydrogen-deuterium exchange mass spectrometry[114]. In summary, MD has proven very useful for the refinement of primary degrader-induced ternary complex simulations yielded by rigid computational approaches.

4.1.2 Analysis techniques

Clustering

Protein-protein docking, ligand conformational sampling, and MD generate a wide repertoire of poses. The large number of structures is sometimes impractical for further analysis steps. In this scenario, clustering can group similar structures and then select (or not) the representative entities (Fig. 3). Many computational pipelines integrate clustering analysis on top of protein-protein docking results. Clustering has also been used to analyze MD simulations[113] in order to categorize the conformational space or to get stable representative poses from the simulations[71, 106, 114-116].

Clustering provides information on structural/conformational frequencies. However, other metrics, such as potential energies, are more useful for assessing the stability of ternary complexes and ΔGs. Docking tools can provide relatively fast calculations, but methods with a higher -computational cost such as MM/GBSA (discussed below) provide more accurate estimations of free energy

Estimating energies with MM/GBSA

Molecular mechanics with generalized Born and surface area solvation (MM/GBSA) is a popular method for calculating free energies in protein-ligand complexes[117-119]. This estimation is obtained by computing the energy difference between bound and unbound states. To this end, the energy of the ligand and the protein in solvent-like conditions is subtracted from that of the protein-ligand complex. First, the system has to be sampled using MD or Monte Carlo (MC) methods. In MC simulations, in contrast to MD, the position and conformations of the ligand are randomly sampled to explore different configurations within the binding site. Regardless of the sampling technique applied, the energy is calculated for all the relevant snapshots in the simulation and the average is used to estimate ΔGs[120] (Fig. 4). MM/GBSA is straightforward but middle-precision approach to compute binding affinities with moderate computational resources[121-122]. Due to the large number of representative conformations produced from protein-protein docking and ligand conformational sampling, the moderate cost of this technique is suitable to estimate energies and evaluate the simulated ternary complexes.

ANM and normal mode analysis

Techniques such as anisotropic network models (ANMs) simplify the protein structure as a network of nodes and edges. Each node in the network denotes a protein residue and the edges represent the bonds between them. Through this simplification, protein flexibility can be studied by the analysis of normal modes[123], which describes the collective motion of the residues. By tracking the changes in normal mode amplitudes over time, ANMs quantify the dynamic behavior of the protein and track large conformational changes (Fig. 3). As discussed in section 4.2.3, the addition of this flexibility permits monitoring of the distance between the E2 and the accessible lysine residues of the POI[124-125] and correlation of these data with experimental degradation.

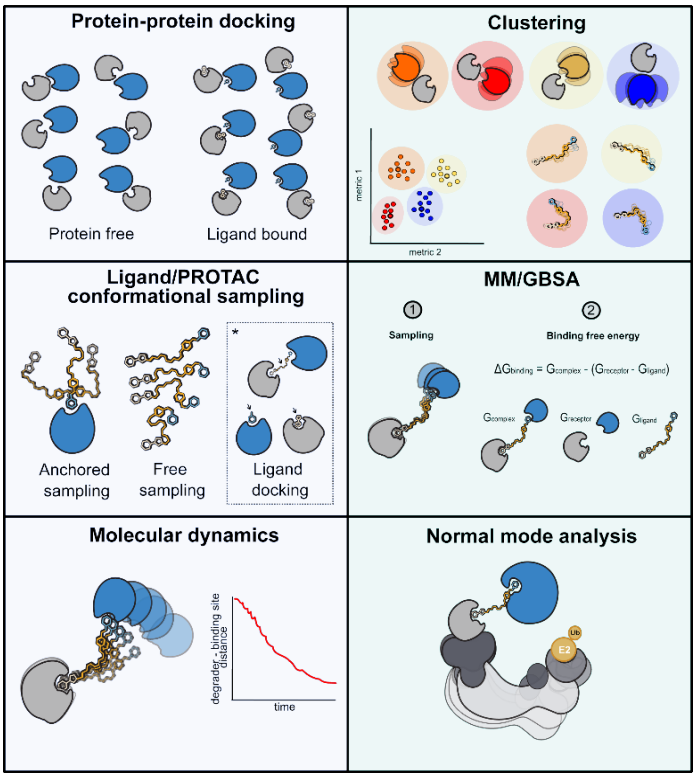

Figure 3. Schematic illustration of the key computational methods applied in TPD. Left: Depiction of the structure generation techniques. Right: Depiction of the analysis methods. For further information about individual techniques, see section 4.1.

4.2 Modeling pipelines in TPD

All the previous techniques can be used separately to guide the design and discovery of degraders. In recent years, more complex computational pipelines have been developed which integrate and combine these techniques to more accurately predict the formation of ternary complexes. Many of these methods have been validated by reproducing known X-ray structures. When such crystals are not available, only degradation and biophysical data can be used to explain the behavior of a given compound. We discuss below some of the most relevant pipelines used in the TPD context.

4.2.1 Docking of ternary complexes

The methods of Drummond *et al.* (2019, 2020)

Drummond *et al.* (2019) reported one of the first in silico modeling pipelines. In that seminal article, they proposed four distinct methods to predict ternary complexes. Method 1 combined protein-protein docking with sampling of the linker between two anchored warheads. During this process, one protein was docked on top of the other and the unconstrained linker bonds were randomly

sampled and re-adapted to fit the new pose (Fig. 4). Method 2 followed a similar strategy, but the PROTAC conformations were freely sampled (Fig. 3 and 4). Ternary complexes were calculated by aligning the warheads on the previous solutions and superposing the protein structures on top of them. Clashing conformations were then discarded (Fig. 4). In Method 3, one of the two PROTAC's warheads was bound to the POI (Fig. 3). The linker conformations were sampled and the second protein was superposed onto these results (Fig. 4). As in Method 2, only non-clashing conformations were considered. Finally, Method 4 was a combination of Methods 2 and 1. It included protein-protein dockings (with both warheads bound) (Fig. 3) and sampling of PROTAC conformations (as in Method 2). The docked poses were overlapped with PROTAC solutions and compatible structures were combined to form ternary complexes (Fig. 4). All methods were assessed on ternary complex crystals of the MZ PROTAC's series of the BET family (BRD2, BRD3, BRD4) on VHL or CRBN E3s[25, 80]. Method 4 outperformed the others[101].

Soon after, the authors extended Method 4 to 4B. In this version, the PROTAC was constrained to keep the bound geometries in the conformational search and a double-clustering strategy was incorporated (Fig. 4)[126]. Overall, Method 4B improved the ability to reproduce X-ray-like ternary complexes, particularly in VHL-based systems compared to CRBN-based systems. The last strategy defined by Drummond et al. (2020) was Method 5. In this version, the linker of the PROTAC spanned between the two proteins from protein-protein docking poses (Fig. 4). However, this method did not show a significant improvement over the double-clustering in Method 4B[126]. There are several examples in the literature of the successful application of these methods to guide the design of PROTACs[101, 106, 127-128].

Rosetta-based pipelines

As mentioned in section 4.1, one of the first computational strategies to guide PROTAC design was reported by Nowak *et al.* (2018)[25]. RosettaDock was applied on lenalidomide-CRBN and JQ1-BRD4^{BD1} to then cluster the results and use structural data to determine the minimal linker length needed to produce productive ternary complexes. They prospectively correlated this data with cellular degradation in BET bromodomains on the PROTACs ZXH-2-147 and ZXH-3-26. Furthermore, they computationally rationalized the specific degradation of ZXH-3-26 to BRD4^{BD1} [25].

PRosettaC is another pioneering pipeline to predict ternary complexes that slowly forces the separation of the two protein-anchoring moieties[96]. At the same time, the linker conformations are randomly sampled by fitting these geometrical constraints. The distribution of accepted

519 conformations is used to determine the range of minimum and maximum PROTAC distances. Global
520 docking with PatchDock and local protein-protein docking refinements with RosettaDock were then
521 performed. Afterward, random linker conformations connect the two PROTAC warheads. Finally,
522 from the lowest Rosetta score conformations, the poses with the best energy in the PPI regions are
523 selected (Fig. 5). Ternary complexes are clustered and ranked according to size. Like the methods
524 devise by Drummond et al., PRosettaC has been successfully used to model initial ternary complexes
525 for further MD (and MM/GBSA rescoring) refinements[115, 125, 129-130].

526 In parallel to the development of the PRosettaC pipeline, Bai *et al.* (2021) executed Rosetta but
527 recycling a protein-protein docking version that was originally developed for antibodies. This strategy
528 requires an initial manually placed complex. Protein-protein docking is performed by refining the
529 given conformation and the top-scored poses are collected for the next step. Then, the warhead
530 portion connecting the linkers, and the linkers themselves are selected and sampled. The generated
531 conformers are aligned with the docked moieties and low RMSD conformers are selected to build the
532 PROTAC. Finally, the complex is refined by minimizing the Rosetta energy function. These ternary
533 complex candidates are filtered by energy and analyzed to get the fraction of fully compatible
534 complexes (Fig. 5). This metric aims to measure how well the PROTAC adapts to the inherent
535 conformational constraints of the ternary complex[131]. In addition, Dixon *et al.* (2022) followed a
536 comparable strategy that enhances the prediction performance of docking routines[132].

537 **FRODOCK and the RosettaDock combination**

538 This new methodology integrates two levels of docking. The first level consists of local protein-protein
539 docking with FRODOCK, where interacting poses are maintained. PROTAC conformations are
540 sampled, internal ligand conformations are rescored and final PROTAC binding energies are assessed
541 and re-ranked based on protein-protein contacts. The results are clustered, and the chosen models
542 are then refined in the second level with RosettaDock (Fig. 4). With this pipeline, near-native
543 conformations were recapitulated from individual crystals, performing significantly better than
544 PRosettaC in 14 case studies[98].

545 ### 4.2.2 MD-based protocols

546 The incorporation of MD into ternary complex modeling was key to improving pipeline predictions.
547 Li *et al.* (2022) proposed a novel strategy relying on MD to re-rank the ternary complexes generated
548 by PRosettaC. They highlighted the effectivity of MM/GBSA calculations to assess the stability and
549 cooperativity of PROTAC-induced ternary complexes (Fig. 4)[129] and correlated these data with

experimental K_d values obtained from biophysical assays. Liao *et al.* (2022) developed another MD-based pipeline integrating protein-protein docking with ligand docking to create starting ternary complex candidates[115]. These structures are refined with MD, clustered and pre-scored with MM/GBSA, and then finally scored with the heating-accelerated pose departure (HAPOD) protocol. Additionally, HAPOD rescoring was proposed on top of PRosettaC-generated ternary complexes, facilitating the identification of near-native poses (Fig. 4)[115]. One of the most prominent examples of MD-based pipelines is the protocol described by Dixon *et al.* (2022)[114]. Starting from separated structures, they used HDX-MS data to approach the formation of the iso2-SMARCA2BD:VHL ternary complex by applying weighted ensemble (WE-HDX) and atomistic Hamiltonian replica-exchange MD (HREMD) simulations (Fig. 4). These millisecond-long simulations revealed the most stable states of $SMARCA2^{BD}$:VHL induced by different degraders (PROTAC1, PROTAC2, and ACBI1)[114].

In summary, incorporating MD into the mentioned workflows improves the quality of ternary complex models. However, the high computational cost of these techniques restricts their application to low-throughput scenarios (a small number of compounds). Faster refinement techniques (e.g., Monte Carlo methods[133-134]) may help reduce the computation expenses and enable the screening of larger numbers of degraders. These techniques use implicit solvent models to accelerate simulations, but this comes at the cost of reduced accuracy.

4.2.3 Models to predict ubiquitination

Protein degradation relies on the ubiquitination of the POI, which requires that the E2 has access to surface lysine residues in the POI. To accurately model the ubiquitin transferring process, recent computational methods have aimed to assemble the entire E3 multisubunit complex. This is done by aligning common subunits based on existing structures determined by X-ray crystallography or Cryo-EMs (or protein-docked solutions)[124-125]. Once the macromodel is complete, different analysis strategies can be applied to identify structural patterns that are associated with ubiquitination processes (Fig. 4). For instance, Dixon *et al.* (2022) also correlated PROTAC-induced ubiquitination with the density of lysines in the ubiquitination zone of $SMARCA2^{BD}$ by superposing the E3 macro-assemble on HREMD results[114]. The aforementioned examples give insights into the importance of tracking the dynamics of the E3 complex in computational models to predict PROTAC-induced ubiquitination and subsequent degradation.

4.2.4 Machine learning-based pipelines

The increasing number of crystallized ternary complexes in the PDB[135] and the degradation data collected by databases such as PROTAC-DB[98, 136] have enabled the application of machine learning strategies in the TPD field. For example, Bayesian Optimization has improved the quality of modeled ternary complex poses on unbound structures[116]. Reinforcement learning algorithms have been implemented to generate PROTACs with improved pharmacokinetic properties. Deep learning has also been applied in methods such as DeepPROTACs to detect the capacity of PROTACs to induce degradation (Fig. 4)[125]. Moreover, machine-learning algorithms have been used to assess the intrinsic degradability of POIs[137], and PROTAC permeability[138-139].

5. Discussion

Computational modeling is gaining momentum within the TPD field to help rationalize degrader design. This trend is evidenced by the growing number of computational pipelines reported[140]. To date, new degraders have been predominantly identified through trial-and-error (PROTACs) and serendipity (MG degraders).

In this review, we have summarized the rapid evolution of computational models to help tackle the challenges posed by the identification of new proximity-inducing agents. The successful application of these methods depends on the availability of robust and high-quality structural and biophysical data. Here we have outlined the range of in vitro and in cellulo approaches used to characterize ternary complex formation and degradation. Initiatives such as the PROTAC-DB have begun to improve accessibility to such data, which will be vital for the advancement of computational strategies. Current efforts in the TPD community to standardize this type of data will greatly facilitate its use as actionable information to drive further advances (e.g., the Chemical Probes Portal offers guidelines[141]).

Research into degrader efficiency has focused mainly on monitoring the degradation of the POI. As a result, an in-depth biophysical analysis of the ternary complex (e.g., kinetics and thermodynamics) is often lacking. Degradation data can be useful to train computer models and improve their predictions. However, using degradation as an output to directly extrapolate ternary complex formation can be misleading[142].

The low number of ternary complexes that have been characterized biophysically and/or structurally currently restricts the power of computational methods. In this regard, CRBN- and VHL-recruiting degraders and ternary complexes involving BET proteins are overrepresented. Furthermore, current computational models have focused solely on the design of PROTACs rather than MG degraders. The

emergence of new structural and biophysical data for MG-induced ternary complex formation may expedite this process.

Finally, we wish to emphasize the critical role of structural and biophysical data in helping computational models achieve accurate degrader designs and better predictions of efficiency. By leveraging these data, computational models have the potential (in the long term) to provide greater insights into the molecular features that govern small molecule-induced ternary complexes in TPD and other proximity-inducing modalities.

Acknowledgements

We would like to thank the members of the Mayor-Ruiz group and A. M. Díaz-Rovira for helpful discussion that helped shape the content of this review. We apologize to the colleagues who could not be cited due to space restriction. The Mayor-Ruiz lab has funding from the European Research Council (ERC) as a Starting Grant to C.M-R. (ERC-2021-StG-101040046 TrickE3), "la Caixa" Foundation, FERO-ASEICA, AECC, the Mark Foundation for Cancer Research, and the Spanish Ministry of Science and Innovation, among others.

Conflict of Interest

C.M-R. is part of the scientific advisory board of Nostrum Biodiscovery. The Mayor-Ruiz laboratory has received or receives sponsored research support from Almirall and Aelin Therapeutics. C. L-P. has a dual part-time affiliation (IRB Barcelona and Nostrum Biodiscovery). The remaining authors report no competing interests.

634

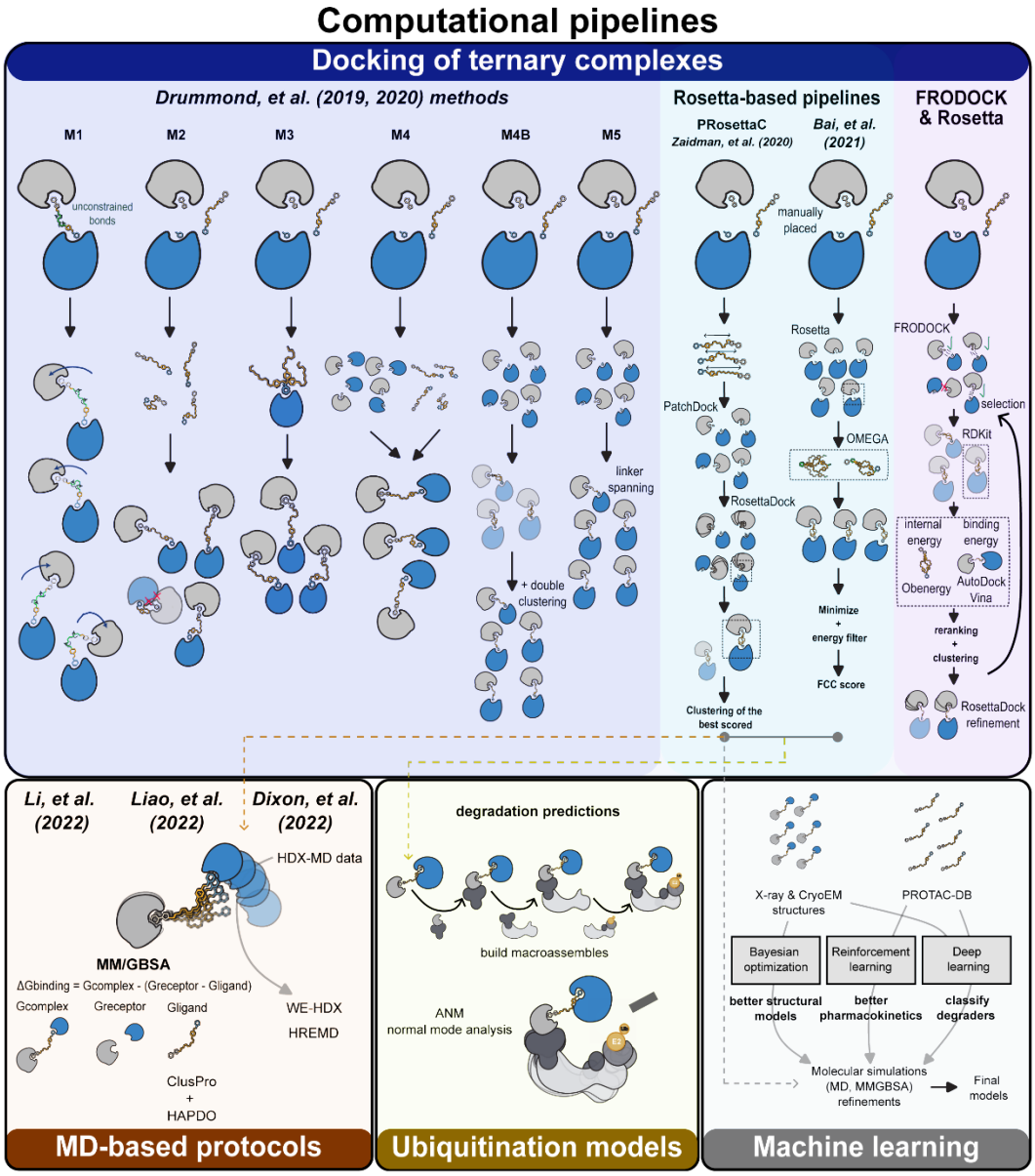

Figure 4. Main computational pipelines applied to PROTAC studies. *For further information about individual pipelines, see section 4.2.*

635 **Keywords**

636 Degraders; biophysical assays; computational strategies; molecular glues; PROTACs.

637

638

639

References

[1] O. Kana, M. Brylinski, *J Comput Aided Mol Des* **2019**, *33*, 509-519.
[2] C. Mayor-Ruiz, G. E. Winter, *Drug Discov Today Technol* **2019**, *31*, 81-90.
[3] M. Bekes, D. R. Langley, C. M. Crews, *Nat Rev Drug Discov* **2022**, *21*, 181-200.
[4] M. Schapira, M. F. Calabrese, A. N. Bullock, C. M. Crews, *Nat Rev Drug Discov* **2019**, *18*, 949-963.
[5] E. Bulatov, A. Ciulli, *Biochem J* **2015**, *467*, 365-386.
[6] A. Domostegui, L. Nieto-Barrado, C. Perez-Lopez, C. Mayor-Ruiz, *Chem Soc Rev* **2022**, *51*, 5498-5517.
[7] L. Nieto-Barrado, A. Domostegui, C. Mayor-Ruiz, in *Inducing Targeted Protein Degradation*, **2023**, pp. 177-204.
[8] W. Farnaby, M. Koegl, D. B. McConnell, A. Ciulli, *Curr Opin Pharmacol* **2021**, *57*, 175-183.
[9] S. Imaide, K. M. Riching, N. Makukhin, V. Vetma, C. Whitworth, S. J. Hughes, N. Trainor, S. D. Mahan, N. Murphy, A. D. Cowan, K. H. Chan, C. Craigon, A. Testa, C. Maniaci, M. Urh, D. L. Daniels, A. Ciulli, *Nat Chem Biol* **2021**, *17*, 1157-1167.
[10] C. A. Lipinski, F. Lombardo, B. W. Dominy, P. J. Feeney, *Adv Drug Deliv Rev* **2001**, *46*, 3-26.
[11] A. Mullard, *Nat Rev Drug Discov* **2021**, *20*, 247-250.
[12] S. Ren, C. Xin, J. Pfeilschifter, A. Huwiler, *Cell Physiol Biochem* **2010**, *26*, 97-104.
[13] H. Rui, K. S. Ashton, J. Min, C. Wang, P. R. Potts, *RSC Chemical Biology* **2023**.
[14] D. M. Sabatini, H. Erdjument-Bromage, M. Lui, P. Tempst, S. H. Snyder, *Cell* **1994**, *78*, 35-43.
[15] M. S. Gadd, A. Testa, X. Lucas, K. H. Chan, W. Chen, D. J. Lamont, M. Zengerle, A. Ciulli, *Nat Chem Biol* **2017**, *13*, 514-521.
[16] C. Maniaci, S. J. Hughes, A. Testa, W. Chen, D. J. Lamont, S. Rocha, D. R. Alessi, R. Romeo, A. Ciulli, *Nat Commun* **2017**, *8*, 830.
[17] K. H. Chan, M. Zengerle, A. Testa, A. Ciulli, *J Med Chem* **2018**, *61*, 504-513.
[18] A. Testa, X. Lucas, G. V. Castro, K. H. Chan, J. E. Wright, A. C. Runcie, M. S. Gadd, W. T. A. Harrison, E. J. Ko, D. Fletcher, A. Ciulli, *J Am Chem Soc* **2018**, *140*, 9299-9313.
[19] X. Han, L. Zhao, W. Xiang, C. Qin, B. Miao, T. Xu, M. Wang, C. Y. Yang, K. Chinnaswamy, J. Stuckey, S. Wang, *J Med Chem* **2019**, *62*, 11218-11231.
[20] A. Zorba, C. Nguyen, Y. Xu, J. Starr, K. Borzilleri, J. Smith, H. Zhu, K. A. Farley, W. Ding, J. Schiemer, X. Feng, J. S. Chang, D. P. Uccello, J. A. Young, C. N. Garcia-Irrizary, L. Czabaniuk, B. Schuff, R. Oliver, J. Montgomery, M. M. Hayward, J. Coe, J. Chen, M. Niosi, S. Luthra, J. C. Shah, A. El-Kattan, X. Qiu, G. M. West, M. C. Noe, V. Shanmugasundaram, A. M. Gilbert, M. F. Brown, M. F. Calabrese, *Proc Natl Acad Sci U S A* **2018**, *115*, E7285-E7292.
[21] V. Zoppi, S. J. Hughes, C. Maniaci, A. Testa, T. Gmaschitz, C. Wieshofer, M. Koegl, K. M. Riching, D. L. Daniels, A. Spallarossa, A. Ciulli, *J Med Chem* **2019**, *62*, 699-726.
[22] R. A. Copeland, *Nat Rev Drug Discov* **2016**, *15*, 87-95.
[23] S. C. Rosenberg, F. Shanahan, S. Yamazoe, M. Kschonsak, Y. J. Zeng, J. Lee, E. Plise, I. Yen, C. M. Rose, J. G. Quinn, L. J. Gazzard, B. T. Walters, D. S. Kirkpatrick, S. T. Staben, S. A. Foster, S. Malek, *Cell Chem Biol* **2023**.
[24] E. S. Wang, A. L. Verano, R. P. Nowak, J. C. Yuan, K. A. Donovan, N. A. Eleuteri, H. Yue, K. H. Ngo, P. H. Lizotte, P. C. Gokhale, N. S. Gray, E. S. Fischer, *Nat Chem Biol* **2021**, *17*, 711-717.
[25] R. P. Nowak, S. L. DeAngelo, D. Buckley, Z. He, K. A. Donovan, J. An, N. Safaee, M. P. Jedrychowski, C. M. Ponthier, M. Ishoey, T. Zhang, J. D. Mancias, N. S. Gray, J. E. Bradner, E. S. Fischer, *Nat Chem Biol* **2018**, *14*, 706-714.

[26] G. E. Winter, A. Mayer, D. L. Buckley, M. A. Erb, J. E. Roderick, S. Vittori, J. M. Reyes, J. di Iulio, A. Souza, C. J. Ott, J. M. Roberts, R. Zeid, T. G. Scott, J. Paulk, K. Lachance, C. M. Olson, S. Dastjerdi, S. Bauer, C. Y. Lin, N. S. Gray, M. A. Kelliher, L. S. Churchman, J. E. Bradner, *Mol Cell* 2017, *67*, 5-18 e19.

[27] R. P. Wurz, K. Dellamaggiore, H. Dou, N. Javier, M. C. Lo, J. D. McCarter, D. Mohl, C. Sastri, J. R. Lipford, V. J. Cee, *J Med Chem* 2018, *61*, 453-461.

[28] G. Du, J. Jiang, N. J. Henning, N. Safaee, E. Koide, R. P. Nowak, K. A. Donovan, H. Yoon, I. You, H. Yue, N. A. Eleuteri, Z. He, Z. Li, H. T. Huang, J. Che, B. Nabet, T. Zhang, E. S. Fischer, N. S. Gray, *Cell Chem Biol* 2022, *29*, 1470-1481 e1431.

[29] K. R. Simonetta, J. Taygerly, K. Boyle, S. E. Basham, C. Padovani, Y. Lou, T. J. Cummins, S. L. Yung, S. K. von Soly, F. Kayser, J. Kuriyan, M. Rape, M. Cardozo, M. A. Gallop, N. F. Bence, P. A. Barsanti, A. Saha, *Nat Commun* 2019, *10*, 1402.

[30] G. Petzold, E. S. Fischer, N. H. Thoma, *Nature* 2016, *532*, 127-130.

[31] C. Mayor-Ruiz, S. Bauer, M. Brand, Z. Kozicka, M. Siklos, H. Imrichova, I. H. Kaltheuner, E. Hahn, K. Seiler, A. Koren, G. Petzold, M. Fellner, C. Bock, A. C. Muller, J. Zuber, M. Geyer, N. H. Thoma, S. Kubicek, G. E. Winter, *Nat Chem Biol* 2021, *17*, 361.

[32] T. B. Faust, H. Yoon, R. P. Nowak, K. A. Donovan, Z. Li, Q. Cai, N. A. Eleuteri, T. Zhang, N. S. Gray, E. S. Fischer, *Nat Chem Biol* 2020, *16*, 7-14.

[33] W. Farnaby, M. Koegl, M. J. Roy, C. Whitworth, E. Diers, N. Trainor, D. Zollman, S. Steurer, J. Karolyi-Oezguer, C. Riedmueller, T. Gmaschitz, J. Wachter, C. Dank, M. Galant, B. Sharps, K. Rumpel, E. Traxler, T. Gerstberger, R. Schnitzer, O. Petermann, P. Greb, H. Weinstabl, G. Bader, A. Zoephel, A. Weiss-Puxbaum, K. Ehrenhofer-Wolfer, S. Wohrle, G. Boehmelt, J. Rinnenthal, H. Arnhof, N. Wiechens, M. Y. Wu, T. Owen-Hughes, P. Ettmayer, M. Pearson, D. B. McConnell, A. Ciulli, *Nat Chem Biol* 2019, *15*, 672-680.

[34] J. F. Glickman, X. Wu, R. Mercuri, C. Illy, B. R. Bowen, Y. He, M. Sills, *J Biomol Screen* 2002, *7*, 3-10.

[35] R. M. Eglen, T. Reisine, P. Roby, N. Rouleau, C. Illy, R. Bossé, M. Bielefeld, *Curr Chem Genomics* 2008, *1*, 2-10.

[36] L. M. Stevers, M. Wolter, G. W. Carlile, D. Macdonald, L. Richard, F. Gielkens, J. W. Hanrahan, D. Y. Thomas, S. K. Chakka, M. L. Peterson, H. Thomas, L. Brunsveld, C. Ottmann, *Nat Commun* 2022, *13*, 3586.

[37] M. Falcicchio, J. A. Ward, S. Y. Chothia, J. Basran, A. Mohindra, S. Macip, P. Roversi, R. G. Doveston, *Chem Sci* 2021, *12*, 12985-12992.

[38] M. J. Roy, S. Winkler, S. J. Hughes, C. Whitworth, M. Galant, W. Farnaby, K. Rumpel, A. Ciulli, *ACS Chem Biol* 2019, *14*, 361-368.

[39] A. Testa, S. J. Hughes, X. Lucas, J. E. Wright, A. Ciulli, *Angew Chem Int Ed Engl* 2020, *59*, 1727-1734.

[40] F. Centorrino, B. Andlovic, P. Cossar, L. Brunsveld, C. Ottmann, *Curr Res Struct Biol* 2022, *4*, 21-28.

[41] M. Slabicki, Z. Kozicka, G. Petzold, Y. D. Li, M. Manojkumar, R. D. Bunker, K. A. Donovan, Q. L. Sievers, J. Koeppel, D. Suchyta, A. S. Sperling, E. C. Fink, J. A. Gasser, L. R. Wang, S. M. Corsello, R. S. Sellar, M. Jan, D. Gillingham, C. Scholl, S. Frohling, T. R. Golub, E. S. Fischer, N. H. Thoma, B. L. Ebert, *Nature* 2020, *585*, 293-297.

[42] L. M. Stevers, C. V. Lam, S. F. Leysen, F. A. Meijer, D. S. van Scheppingen, R. M. de Vries, G. W. Carlile, L. G. Milroy, D. Y. Thomas, L. Brunsveld, C. Ottmann, *Proc Natl Acad Sci U S A* 2016, *113*, E1152-1161.

[43] D. E. Bussiere, L. Xie, H. Srinivas, W. Shu, A. Burke, C. Be, J. Zhao, A. Godbole, D. King, R. G. Karki, V. Hornak, F. Xu, J. Cobb, N. Carte, A. O. Frank, A. Frommlet, P. Graff, M. Knapp, A.

Fazal, B. Okram, S. Jiang, P. Y. Michellys, R. Beckwith, H. Voshol, C. Wiesmann, J. M. Solomon, J. Paulk, *Nat Chem Biol* 2020, *16*, 15-23.
[44] S. L. Fisher, A. J. Phillips, *Curr Opin Chem Biol* 2018, *44*, 47-55.
[45] H. Connaris, P. R. Crocker, G. L. Taylor, *J Biol Chem* 2009, *284*, 7339-7351.
[46] T. H. Pillow, P. Adhikari, R. A. Blake, J. Chen, G. Del Rosario, G. Deshmukh, I. Figueroa, K. E. Gascoigne, A. V. Kamath, S. Kaufman, T. Kleinheinz, K. R. Kozak, B. Latifi, D. D. Leipold, C. Sing Li, R. Li, M. M. Mulvihill, A. O'Donohue, R. K. Rowntree, J. D. Sadowsky, J. Wai, X. Wang, C. Wu, Z. Xu, H. Yao, S. F. Yu, D. Zhang, R. Zang, H. Zhang, H. Zhou, X. Zhu, P. S. Dragovich, *ChemMedChem* 2020, *15*, 17-25.
[47] C. Kofink, N. Trainor, B. Mair, S. Wohrle, M. Wurm, N. Mischerikow, M. J. Roy, G. Bader, P. Greb, G. Garavel, E. Diers, R. McLennan, C. Whitworth, V. Vetma, K. Rumpel, M. Scharnweber, J. E. Fuchs, T. Gerstberger, Y. Cui, G. Gremel, P. Chetta, S. Hopf, N. Budano, J. Rinnenthal, G. Gmaschitz, M. Mayer, M. Koegl, A. Ciulli, H. Weinstabl, W. Farnaby, *Nat Commun* 2022, *13*, 5969.
[48] B. E. Smith, S. L. Wang, S. Jaime-Figueroa, A. Harbin, J. Wang, B. D. Hamman, C. M. Crews, *Nat Commun* 2019, *10*, 131.
[49] X. Guillory, M. Wolter, S. Leysen, J. F. Neves, A. Kuusk, S. Genet, B. Somsen, J. K. Morrow, E. Rivers, L. van Beek, J. Patel, R. Goodnow, H. Schoenherr, N. Fuller, Q. Cao, R. G. Doveston, L. Brunsveld, M. R. Arkin, P. Castaldi, H. Boyd, I. Landrieu, H. Chen, C. Ottmann, *J Med Chem* 2020, *63*, 6694-6707.
[50] A. M. Hartman, W. A. M. Elgaher, N. Hertrich, S. A. Andrei, C. Ottmann, A. K. H. Hirsch, *ACS Med Chem Lett* 2020, *11*, 1041-1046.
[51] J. Schiemer, R. Horst, Y. Meng, J. I. Montgomery, Y. Xu, X. Feng, K. Borzilleri, D. P. Uccello, C. Leverett, S. Brown, Y. Che, M. F. Brown, M. M. Hayward, A. M. Gilbert, M. C. Noe, M. F. Calabrese, *Nat Chem Biol* 2021, *17*, 152-160.
[52] S. Cao, S. Kang, H. Mao, J. Yao, L. Gu, N. Zheng, *Nat Commun* 2022, *13*, 815.
[53] W. L. Petrilli, G. C. Adam, R. S. Erdmann, P. Abeywickrema, V. Agnani, X. Ai, J. Baysarowich, N. Byrne, J. P. Caldwell, W. Chang, E. DiNunzio, Z. Feng, R. Ford, S. Ha, Y. Huang, B. Hubbard, J. M. Johnston, M. Kavana, J. M. Lisnock, R. Liang, J. Lu, Z. Lu, J. Meng, P. Orth, O. Palyha, G. Parthasarathy, S. P. Salowe, S. Sharma, J. Shipman, S. M. Soisson, A. Strack, H. Youm, K. Zhao, D. L. Zink, H. Zokian, G. H. Addona, K. Akinsanya, J. R. Tata, Y. Xiong, J. E. Imbriglio, *Cell Chem Biol* 2021, *28*, 243.
[54] Q. Zhao, C. Ren, L. Liu, J. Chen, Y. Shao, N. Sun, R. Sun, Y. Kong, X. Ding, X. Zhang, Y. Xu, B. Yang, Q. Yin, X. Yang, B. Jiang, *J Med Chem* 2019, *62*, 9281-9298.
[55] T. Bartoschik, A. Zoephel, K. Rumpel, A. Ciulli, C. Heffern, *Methods Mol Biol* 2021, *2365*, 115-133.
[56] R. Beveridge, D. Kessler, K. Rumpel, P. Ettmayer, A. Meinhart, T. Clausen, *ACS Cent Sci* 2020, *6*, 1223-1230.
[57] J. Bellamy-Carter, M. Mohata, M. Falcicchio, J. Basran, Y. Higuchi, R. G. Doveston, A. C. Leney, *Chem Sci* 2021, *12*, 10724-10731.
[58] D. N. Kenanova, E. J. Visser, J. M. Virta, E. Sijbesma, F. Centorrino, H. R. Vickery, M. Zhong, R. J. Neitz, L. Brunsveld, C. Ottmann, M. R. Arkin, *bioRxiv* 2023, 2023.2001.2029.526112.
[59] G. V. de Castro, A. Ciulli, *RSC Med Chem* 2022, *13*, 98.
[60] K. M. Riching, S. Mahan, C. R. Corona, M. McDougall, J. D. Vasta, M. B. Robers, M. Urh, D. L. Daniels, *ACS Chem Biol* 2018, *13*, 2758-2770.
[61] S. Khan, X. Zhang, D. Lv, Q. Zhang, Y. He, P. Zhang, X. Liu, D. Thummuri, Y. Yuan, J. S. Wiegand, J. Pei, W. Zhang, A. Sharma, C. R. McCurdy, V. M. Kuruvilla, N. Baran, A. A. Ferrando, Y. M.

781 Kim, A. Rogojina, P. J. Houghton, G. Huang, R. Hromas, M. Konopleva, G. Zheng, D. Zhou, *Nat*
782 *Med* 2019, *25*, 1938-1947.
783 [62] S. D. Mahan, K. M. Riching, M. Urh, D. L. Daniels, *Methods Mol Biol* 2021, *2365*, 151-171.
784 [63] J. W. Mason, L. Hudson, M. V. Westphal, A. Tutter, G. Michaud, W. Shu, X. Ma, C. W. Coley,
785 P. A. Clemons, S. Bonazzi, F. Berst, F. J. Zécri, K. Briner, S. L. Schreiber, *bioRxiv* 2022,
786 2022.2010.2013.512184.
787 [64] C. I. Chung, Q. Zhang, X. Shu, *Anal Chem* 2018, *90*, 14287-14293.
788 [65] T. Kaji, H. Koga, M. Kuroha, T. Akimoto, K. Hayata, *Sci Rep* 2020, *10*, 3088.
789 [66] M. C. Silva, F. M. Ferguson, Q. Cai, K. A. Donovan, G. Nandi, D. Patnaik, T. Zhang, H. T. Huang,
790 D. E. Lucente, B. C. Dickerson, T. J. Mitchison, E. S. Fischer, N. S. Gray, S. J. Haggarty, *Elife*
791 2019, *8*.
792 [67] A. L. Chernobrovkin, C. Cazares-Korner, T. Friman, I. M. Caballero, D. Amadio, D. Martinez
793 Molina, *SLAS Discov* 2021, *26*, 534-546.
794 [68] E. Luchinat, L. Barbieri, M. Cremonini, A. Nocentini, C. T. Supuran, L. Banci, *Angew Chem Int*
795 *Ed Engl* 2020, *59*, 6535-6539.
796 [69] J. M. Dubach, E. Kim, K. Yang, M. Cuccarese, R. J. Giedt, L. G. Meimetis, C. Vinegoni, R.
797 Weissleder, *Nat Chem Biol* 2017, *13*, 168-173.
798 [70] N. C. Dale, E. K. M. Johnstone, C. W. White, K. D. G. Pfleger, *Front Bioeng Biotechnol* 2019, *7*,
799 56.
800 [71] A. S. Dixon, M. K. Schwinn, M. P. Hall, K. Zimmerman, P. Otto, T. H. Lubben, B. L. Butler, B. F.
801 Binkowski, T. Machleidt, T. A. Kirkland, M. G. Wood, C. T. Eggers, L. P. Encell, K. V. Wood, *ACS*
802 *Chem Biol* 2016, *11*, 400-408.
803 [72] M. Brand, B. Jiang, S. Bauer, K. A. Donovan, Y. Liang, E. S. Wang, R. P. Nowak, J. C. Yuan, T.
804 Zhang, N. Kwiatkowski, A. C. Muller, E. S. Fischer, N. S. Gray, G. E. Winter, *Cell Chem Biol* 2019,
805 *26*, 300-306 e309.
806 [73] F. Yang, Y. Tan, C. Wu, L. Xin, Z. Huang, H. Zhou, F. Zhou, *Chembiochem* 2023, *24*,
807 e202200680.
808 [74] C. Banning, J. Votteler, D. Hoffmann, H. Koppensteiner, M. Warmer, R. Reimer, F. Kirchhoff,
809 U. Schubert, J. Hauber, M. Schindler, *PLoS One* 2010, *5*, e9344.
810 [75] A. Margineanu, J. J. Chan, D. J. Kelly, S. C. Warren, D. Flatters, S. Kumar, M. Katan, C. W.
811 Dunsby, P. M. French, *Sci Rep* 2016, *6*, 28186.
812 [76] Y. J. Shyu, C. D. Suarez, C. D. Hu, *Nat Protoc* 2008, *3*, 1693-1702.
813 [77] L. A. Serebryannyy, T. Misteli, *Methods* 2019, *157*, 80-87.
814 [78] B. R. Bellenie, K. J. Cheung, A. Varela, O. A. Pierrat, G. W. Collie, G. M. Box, M. D. Bright, S.
815 Gowan, A. Hayes, M. J. Rodrigues, K. N. Shetty, M. Carter, O. A. Davis, A. T. Henley, P.
816 Innocenti, L. D. Johnson, M. Liu, S. de Klerk, Y. V. Le Bihan, M. G. Lloyd, P. C. McAndrew, E.
817 Shehu, R. Talbot, H. L. Woodward, R. Burke, V. Kirkin, R. L. M. van Montfort, F. I. Raynaud, O.
818 W. Rossanese, S. Hoelder, *J Med Chem* 2020, *63*, 4047-4068.
819 [79] N. C. Payne, S. Maksoud, B. A. Tannous, R. Mazitschek, *Cell Chem Biol* 2022, *29*, 1333-1340
820 e1335.
821 [80] M. Zengerle, K. H. Chan, A. Ciulli, *ACS Chem Biol* 2015, *10*, 1770-1777.
822 [81] D. L. Buckley, K. Raina, N. Darricarrere, J. Hines, J. L. Gustafson, I. E. Smith, A. H. Miah, J. D.
823 Harling, C. M. Crews, *ACS Chem Biol* 2015, *10*, 1831-1837.
824 [82] V. Koduri, L. Duplaquet, B. L. Lampson, A. C. Wang, A. H. Sabet, M. Ishoey, J. Paulk, M. Teng,
825 I. S. Harris, J. E. Endress, X. Liu, E. Dasilva, J. A. Paulo, K. J. Briggs, J. G. Doench, C. J. Ott, T.
826 Zhang, K. A. Donovan, E. S. Fischer, S. P. Gygi, N. S. Gray, J. Bradner, J. A. Medin, S. J. Buhrlage,
827 M. G. Oser, W. G. Kaelin, Jr., *Sci Adv* 2021, *7*.

[83] M. P. Schwalm, A. Krämer, A. Dölle, J. Weckesser, X. Yu, J. Jin, K. Saxena, S. Knapp, *bioRxiv* 2023, 2023.2001.2011.523589.

[84] O. Hsia, M. Hinterndorfer, A. D. Cowan, K. Iso, T. Ishida, R. Sundaramoorthy, M. A. Nakasone, A. Rukavina, K. Husnjak, M. Wegner, A. Correa-Sáez, C. Craigon, C. Maniaci, A. Testa, M. Kaulich, I. Dikic, G. E. Winter, A. Ciulli, *bioRxiv* 2023, 2023.2002.2014.528511.

[85] Y.-D. Li, M. W. Ma, M. M. Hassan, M. Hunkeler, M. Teng, K. Puvar, R. Lumpkin, B. Sandoval, C. Y. Jin, S. B. Ficarro, M. Y. Wang, S. Xu, B. J. Groendyke, L. H. Sigua, I. Tavares, C. Zou, J. M. Tsai, P. M. C. Park, H. Yoon, F. C. Majewski, J. A. Marto, J. Qi, R. P. Nowak, K. A. Donovan, M. Słabicki, N. S. Gray, E. S. Fischer, B. L. Ebert, *bioRxiv* 2023, 2023.2002.2014.528208.

[86] Y. Lee, J. Heo, H. Jeong, K. T. Hong, D. H. Kwon, M. H. Shin, M. Oh, G. A. Sable, G. O. Ahn, J. S. Lee, H. K. Song, H. S. Lim, *Angew Chem Int Ed Engl* 2020, *59*, 17548-17555.

[87] J. Jumper, R. Evans, A. Pritzel, T. Green, M. Figurnov, O. Ronneberger, K. Tunyasuvunakool, R. Bates, A. Zidek, A. Potapenko, A. Bridgland, C. Meyer, S. A. A. Kohl, A. J. Ballard, A. Cowie, B. Romera-Paredes, S. Nikolov, R. Jain, J. Adler, T. Back, S. Petersen, D. Reiman, E. Clancy, M. Zielinski, M. Steinegger, M. Pacholska, T. Berghammer, S. Bodenstein, D. Silver, O. Vinyals, A. W. Senior, K. Kavukcuoglu, P. Kohli, D. Hassabis, *Nature* 2021, *596*, 583-589.

[88] M. Baek, F. DiMaio, I. Anishchenko, J. Dauparas, S. Ovchinnikov, G. R. Lee, J. Wang, Q. Cong, L. N. Kinch, R. D. Schaeffer, C. Millan, H. Park, C. Adams, C. R. Glassman, A. DeGiovanni, J. H. Pereira, A. V. Rodrigues, A. A. van Dijk, A. C. Ebrecht, D. J. Opperman, T. Sagmeister, C. Buhlheller, T. Pavkov-Keller, M. K. Rathinaswamy, U. Dalwadi, C. K. Yip, J. E. Burke, K. C. Garcia, N. V. Grishin, P. D. Adams, R. J. Read, D. Baker, *Science* 2021, *373*, 871-876.

[89] R. Evans, M. O'Neill, A. Pritzel, N. Antropova, A. Senior, T. Green, A. Žídek, R. Bates, S. Blackwell, J. Yim, O. Ronneberger, S. Bodenstein, M. Zielinski, A. Bridgland, A. Potapenko, A. Cowie, K. Tunyasuvunakool, R. Jain, E. Clancy, P. Kohli, J. Jumper, D. Hassabis, *bioRxiv* 2021, 2021.2010.2004.463034.

[90] R. Oliva, E. Chermak, L. Cavallo, *Molecules* 2015, *20*, 12045-12060.

[91] A. A. Kaczor, D. Bartuzi, T. M. Stepniewski, D. Matosiuk, J. Selent, *Methods Mol Biol* 2018, *1762*, 285-305.

[92] I. A. Vakser, *Biophys J* 2014, *107*, 1785-1793.

[93] C. Dominguez, R. Boelens, A. M. Bonvin, *J Am Chem Soc* 2003, *125*, 1731-1737.

[94] M. Schiedel, D. Herp, S. Hammelmann, S. Swyter, A. Lehotzky, D. Robaa, J. Olah, J. Ovadi, W. Sippl, M. Jung, *J Med Chem* 2018, *61*, 482-491.

[95] J. J. Gray, S. Moughon, C. Wang, O. Schueler-Furman, B. Kuhlman, C. A. Rohl, D. Baker, *Journal of Molecular Biology* 2003, *331*, 281-299.

[96] D. Zaidman, J. Prilusky, N. London, *J Chem Inf Model* 2020, *60*, 4894-4903.

[97] D. Schneidman-Duhovny, Y. Inbar, R. Nussinov, H. J. Wolfson, *Nucleic Acids Research* 2005, *33*, W363-W367.

[98] G. Weng, D. Li, Y. Kang, T. Hou, *Journal of Medicinal Chemistry* 2021, *64*, 16271-16281.

[99] E. Ramírez-Aportela, J. R. López-Blanco, P. Chacón, *Bioinformatics* 2016, *32*, 2386-2388.

[100] M. L. Drummond, C. I. Williams, *J Chem Inf Model* 2019, *59*, 1634-1644.

[101] M. L. Drummond, A. Henry, H. Li, C. I. Williams, *J Chem Inf Model* 2020, *60*, 5234-5254.

[102] A. Dolle, B. Adhikari, A. Kramer, J. Weckesser, N. Berner, L. M. Berger, M. Diebold, M. M. Szewczyk, D. Barsyte-Lovejoy, C. H. Arrowsmith, J. Gebel, F. Lohr, V. Dotsch, M. Eilers, S. Heinzlmeir, B. Kuster, C. Sotriffer, E. Wolf, S. Knapp, *J Med Chem* 2021, *64*, 10682-10710.

[103] S. S. W. Chemical Computing Group ULC, Suite #910, Montreal, QC, Canada, H3A 2R7, 2023.

[104] D. Kozakov, D. R. Hall, B. Xia, K. A. Porter, D. Padhorny, C. Yueh, D. Beglov, S. Vajda, *Nature Protocols* 2017, *12*, 255-278.

[105] G. P. Pereira, B. Jiménez-García, R. Pellarin, G. Launay, S. Wu, J. Martin, P. C. T. Souza, *bioRxiv* 2023, 2023.2002.2016.528819.

[106] C. L. Zhu, X. Luo, T. Tian, Z. Rao, H. Wang, Z. Zhou, T. Mi, D. Chen, Y. Xu, Y. Wu, J. Che, Y. Zhou, J. Li, X. Dong, *Eur J Med Chem* 2022, *238*, 114459.

[107] S. A. Hollingsworth, R. O. Dror, *Neuron* 2018, *99*, 1129-1143.

[108] X. Liu, D. Shi, S. Zhou, H. Liu, H. Liu, X. Yao, *Expert Opin Drug Discov* 2018, *13*, 23-37.

[109] S. Mansoor, G. Kayık, S. Durdagi, O. Sensoy, *Computational and Structural Biotechnology Journal* 2022, *20*, 925-936.

[110] C. K. Arnatt, B. A. Falls, Y. Yuan, T. J. Raborg, R. R. Masvekar, N. El-Hage, D. E. Selley, A. V. Nicola, P. E. Knapp, K. F. Hauser, Y. Zhang, *Bioorganic & Medicinal Chemistry* 2016, *24*, 5969-5987.

[111] L. Pérez-Benito, A. Henry, M.-T. Matsoukas, L. Lopez, D. Pulido, M. Royo, A. Cordomí, G. Tresadern, L. Pardo, *Bioinformatics* 2018, *34*, 3857-3863.

[112] D. P. Bondeson, B. E. Smith, G. M. Burslem, A. D. Buhimschi, J. Hines, S. Jaime-Figueroa, J. Wang, B. D. Hamman, A. Ishchenko, C. M. Crews, *Cell Chem Biol* 2018, *25*, 78-87 e75.

[113] D. Weerakoon, R. J. Carbajo, L. De Maria, C. Tyrchan, H. Zhao, *J Chem Inf Model* 2022, *62*, 340-349.

[114] T. Dixon, D. MacPherson, B. Mostofian, T. Dauzhenka, S. Lotz, D. McGee, S. Shechter, U. R. Shrestha, R. Wiewiora, Z. A. McDargh, F. Pei, R. Pal, J. V. Ribeiro, T. Wilkerson, V. Sachdeva, N. Gao, S. Jain, S. Sparks, Y. Li, A. Vinitsky, X. Zhang, A. M. Razavi, I. Kolossvary, J. Imbriglio, A. Evdokimov, L. Bergeron, W. Zhou, J. Adhikari, B. Ruprecht, A. Dickson, H. Xu, W. Sherman, J. A. Izaguirre, *Nat Commun* 2022, *13*, 5884.

[115] J. Liao, X. Nie, I. C. Unarta, S. S. Ericksen, W. Tang, *J Med Chem* 2022, *65*, 6116-6132.

[116] A. Rao, T. M. Tunjic, M. Brunsteiner, M. Müller, H. Fooladi, N. Weber, *bioRxiv* 2022, 2022.2006.2003.494737.

[117] J. Srinivasan, J. Miller, P. A. Kollman, D. A. Case, *J Biomol Struct Dyn* 1998, *16*, 671-682.

[118] P. A. Kollman, I. Massova, C. Reyes, B. Kuhn, S. Huo, L. Chong, M. Lee, T. Lee, Y. Duan, W. Wang, O. Donini, P. Cieplak, J. Srinivasan, D. A. Case, T. E. Cheatham, 3rd, *Acc Chem Res* 2000, *33*, 889-897.

[119] J. Srinivasan, T. E. Cheatham, P. Cieplak, P. A. Kollman, D. A. Case, *Journal of the American Chemical Society* 1998, *120*, 9401-9409.

[120] E. Wang, H. Sun, J. Wang, Z. Wang, H. Liu, J. Z. H. Zhang, T. Hou, *Chem Rev* 2019, *119*, 9478-9508.

[121] S. Genheden, U. Ryde, *Expert Opin Drug Discov* 2015, *10*, 449-461.

[122] T. Tuccinardi, *Expert Opinion on Drug Discovery* 2021, *16*, 1233-1237.

[123] V. Alexandrov, U. Lehnert, N. Echols, D. Milburn, D. Engelman, M. Gerstein, *Protein Sci* 2005, *14*, 633-643.

[124] D. Lv, P. Pal, X. Liu, Y. Jia, D. Thummuri, P. Zhang, W. Hu, J. Pei, Q. Zhang, S. Zhou, S. Khan, X. Zhang, N. Hua, Q. Yang, S. Arango, W. Zhang, D. Nayak, S. K. Olsen, S. T. Weintraub, R. Hromas, M. Konopleva, Y. Yuan, G. Zheng, D. Zhou, *Nat Commun* 2021, *12*, 6896.

[125] N. Bai, K. M. Riching, A. Makaju, H. Wu, T. M. Acker, S. C. Ou, Y. Zhang, X. Shen, D. N. Bulloch, H. Rui, B. W. Gibson, D. L. Daniels, M. Urh, B. M. Rock, S. C. Humphreys, *J Biol Chem* 2022, *298*, 101653.

[126] M. L. Drummond, A. Henry, H. Li, C. I. Williams, *Journal of Chemical Information and Modeling* 2020, *60*, 5234-5254.

[127] Y. Murakami, H. Osawa, T. Kurohara, Y. Yanase, T. Ito, H. Yokoo, N. Shibata, M. Naito, K. Aritake, Y. Demizu, *RSC Med Chem* 2022, *13*, 1495-1503.

[128] T. Niu, K. Li, L. Jiang, Z. Zhou, J. Hong, X. Chen, X. Dong, Q. He, J. Cao, B. Yang, C. L. Zhu, *Eur J Med Chem* **2022**, *228*, 114012.
[129] W. Li, J. Zhang, L. Guo, Q. Wang, *J Chem Inf Model* **2022**, *62*, 523-532.
[130] S. Zheng, Y. Tan, Z. Wang, C. Li, Z. Zhang, X. Sang, H. Chen, Y. Yang, *Nature Machine Intelligence* **2022**, *4*, 739-748.
[131] N. Bai, S. A. Miller, G. V. Andrianov, M. Yates, P. Kirubakaran, J. Karanicolas, *J Chem Inf Model* **2021**, *61*, 1368-1382.
[132] T. Dixon, D. MacPherson, B. Mostofian, T. Dauzhenka, S. Lotz, D. McGee, S. Shechter, U. R. Shrestha, R. Wiewiora, Z. A. McDargh, F. Pei, R. Pal, J. V. Ribeiro, T. Wilkerson, V. Sachdeva, N. Gao, S. Jain, S. Sparks, Y. Li, A. Vinitsky, X. Zhang, A. M. Razavi, I. Kolossváry, J. Imbriglio, A. Evdokimov, L. Bergeron, W. Zhou, J. Adhikari, B. Ruprecht, A. Dickson, H. Xu, W. Sherman, J. A. Izaguirre, *Nature Communications* **2022**, *13*, 5884.
[133] K. W. Borrelli, A. Vitalis, R. Alcantara, V. Guallar, *Journal of Chemical Theory and Computation* **2005**, *1*, 1304-1311.
[134] W. L. Jorgensen, J. Tirado-Rives, *J Comput Chem* **2005**, *26*, 1689-1700.
[135] H. M. Berman, J. Westbrook, Z. Feng, G. Gilliland, T. N. Bhat, H. Weissig, I. N. Shindyalov, P. E. Bourne, *Nucleic Acids Res* **2000**, *28*, 235-242.
[136] G. Weng, X. Cai, D. Cao, H. Du, C. Shen, Y. Deng, Q. He, B. Yang, D. Li, T. Hou, *Nucleic Acids Res* **2023**, *51*, D1367-D1372.
[137] W. Zhang, S. S. Roy Burman, J. Chen, K. A. Donovan, Y. Cao, C. Shu, B. Zhang, Z. Zeng, S. Gu, Y. Zhang, D. Li, E. S. Fischer, C. Tokheim, X. Shirley Liu, *Genomics Proteomics Bioinformatics* **2022**.
[138] V. Poongavanam, F. Kölling, A. Giese, A. H. Göller, L. Lehmann, D. Meibom, J. Kihlberg, *ACS Omega* **2023**, *8*, 5901-5916.
[139] V. Poongavanam, Y. Atilaw, S. Siegel, A. Giese, L. Lehmann, D. Meibom, M. Erdelyi, J. Kihlberg, *Journal of Medicinal Chemistry* **2022**, *65*, 13029-13040.
[140] M. Ignatov, A. Jindal, S. Kotelnikov, D. Beglov, G. Posternak, X. Tang, P. Maisonneuve, G. Poda, R. A. Batey, F. Sicheri, A. Whitty, P. J. Tonge, S. Vajda, D. Kozakov, *Journal of the American Chemical Society* **2023**.
[141] A. A. Antolin, D. Sanfelice, A. Crisp, E. Villasclaras Fernandez, I. L. Mica, Y. Chen, I. Collins, A. Edwards, S. Muller, B. Al-Lazikani, P. Workman, *Nucleic Acids Res* **2023**, *51*, D1492-D1502.
[142] D. Park, J. Izaguirre, R. Coffey, H. Xu, *ACS Bio & Med Chem Au* **2023**, *3*, 74-86.

Table of contents entry

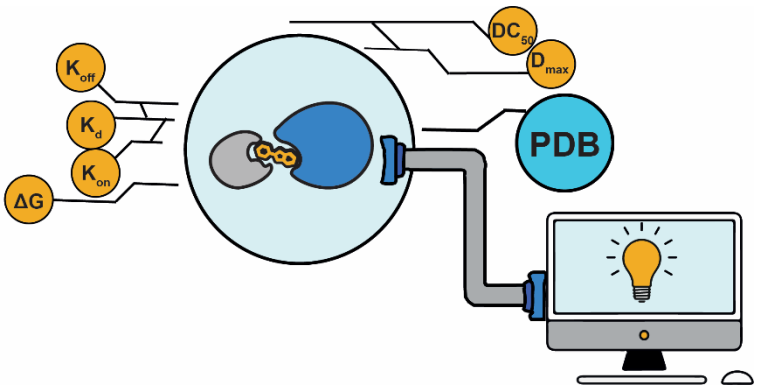

A comprehensive review of biophysical and computational methodology used in the targeted protein

958 degradation field, emphasizing the importance of high-quality data for the accurate computation of
959 degrader-induced ternary complex models.

960

961 **Twitter**

962 @CrisMayorRuiz @IRBBarcelona

963